

CHARACTERIZATION OF THE MECHANICAL PROPERTIES OF PLASMA-SPRAYED COATINGS

N.R. Shankar, C.C. Berndt and H. Herman

Dept. of Materials Science & Engineering
State University of New York
Stony Brook, N.Y. 11794

ABSTRACT

The heterogeneous nature of plasma-sprayed coatings plays a major role in their mechanical properties. The fundamental deformation modes are usually classified as adhesive or cohesive. However, these failure mechanisms are poorly understood, especially when they are related to coating performance under service conditions.

Strain deformation of plasma-sprayed stainless steel and yttria-stabilized zirconia coatings, with and without a NiCrAlY bond coat, were measured and the acoustic emission (AE) generated during the test was simultaneously monitored. Comparison of the results with coatings heat treated for 10 hours at 1150°C and stainless steel coatings showed that AE correlates with the fracture mode. Heat treatment affected the bond strength and also the type of fracture. Coating and fracture characterization by SEM and EDA, coupled with AE results, show potential for studying coating adhesion and integrity.

INTRODUCTION

The failure mechanisms of plasma-sprayed ceramic coatings are not completely understood. The response of a coating system to mechanical and thermal stresses is influenced by a highly oriented microstructure and by the incorporation of an intermediate bond coat^{1,2,3}.

The durability of coatings depends both on coating properties and, more fundamentally, on their adhesion strength to the substrate. The adhesion of coatings is conventionally determined by the Tensile Adhesion Test, ASTM C633-69 (TAT)⁴. The end of a 25mm diameter rod is coated and then epoxied to a like rod (support bar), thus forming a tensile specimen. If the epoxy has a tensile strength greater than that of the adhesion strength, the latter can be determined by a tensile test.

The TAT results, due to both the nature of the test and the coating microstructure, exhibit wide scatter^{5,6}. Also, coating failures often show both cohesive and adhesive fracture regions and, therefore, characterization of the bond strength by a single number is not realistic and, furthermore, does not lead to an understanding of coating failure mechanisms.

In this study, the TAT was coupled with the technique of Acoustic Emission (AE)⁷ in order to study coating failure. AE, in the present context, refers to elastic waves arising due to the generation and propagation of cracks. Previous work done on ZrO₂-8 wt% Y₂O₃ plasma-sprayed coatings showed that AE can, in fact, differentiate between failure mechanisms and that cumulative AE counts can be correlated with bond strength⁸.

This paper describes similar tests performed on ZrO₂-7 wt% Y₂O₃ coatings, with and without a NiCrAlY bond coat. Coatings were tested in as-sprayed and heat-treated conditions and contrasted with stainless steel coatings. Coatings were subjected to repeated, increasing loading until rupture occurred.

EXPERIMENTAL PROCEDURE

Yttria-stabilized zirconia (YSZ), with and without a NiCrAlY bond coat, and stainless steel were plasma sprayed onto ends of cylindrical steel substrates conforming to specifications of ASTM Tensile Adhesion Test C633-69. Prior to plasma spraying, the substrate surface was prepared by grit blasting. The average deposit thickness of the stainless steel metallic coating was 0.4mm and that of the ceramic coating was 0.5mm. Experimental details of plasma spraying and the heat treatment procedure have been described previously⁸. Following the heat treatment, the coatings were furnace cooled to room temperature.

YSZ powder was also plasma sprayed into water using the same spray parameters as that used to produce the coatings. This was done to characterize the effect of the plasma effluent on powder shape, distribution, and degree of melting. Particle size distribution of all the powders was determined by sieving in 7.5cm diameter sieves of woven copper.

The experimental arrangement of AE monitoring during TAT and specimen preparation technique have been described in a previous publication⁸. A special TAT jig has been constructed with a flat face on the support bar, which allows the attachment of the AE transducer. As the tensile load is applied, cohesive (through the coating) and/or adhesive (through the coating-substrate interface), failure occur(s). The propagating cracks give rise to acoustic signals which is detected and registered by the AE setup. The output from the AE transducer was amplified to 80 dB gain. The amplified voltage was then compared with an automatic threshold voltage (which compensates for background and system noise), and each crossing of this threshold voltage was counted by the signal processor as a ring-down count. Also monitored was the RMS voltage, which is related to the intensity of the generated AE, and the AE events, which represent each acoustic pulse. The force vs extension curve was plotted and some specimens were: (i) subjected to repeated loadings; and (ii) held at certain loads before being loaded to rupture.

The powders, sprayed surfaces and the fracture surfaces of the coatings were examined by scanning electron microscopy (SEM) and by energy dispersive analysis (EDA). Fracture surfaces of both the substrate and support bar pieces were also examined by optical stereomicroscopy to characterize the fracture on a macroscopic scale.

RESULTS

Powder and Coating Characterization

SEM's of the YSZ powder are shown in both the as-received and water-quenched conditions in Fig. 1 and their characteristics are listed in Table I. Fig. 1d, for water-quenched YSZ, shows a large amount of partially molten particles and microcracking. Water quenching of YSZ did not significantly alter the particle size distribution. Both of the as-received metallic powders, on the other hand, exhibited much narrower size ranges.

The surfaces of the metallic coatings revealed more particle spreading than the case of the ceramic coatings; while the latter also exhibited more cracking. Surface cracks in the YSZ coatings increased in number and length with heat treatment; particularly for the duplex coating have a NiCrAlY bond coat. X-ray diffraction of the heat-treated YSZ coating revealed a slight increase in the tetragonal to cubic phase ratio. Heat treatment of the YSZ + NiCrAlY coating modified the coating color from yellow to gray indicating a slight change in the stoichiometry of the oxide. EDA analysis of the oxide coating surface showed the absence of Ni, Cr and Al; while the presence of Y was masked by the Zr peak.

Table I. Powder Characteristics

Powder	Composition wt %	Size Range μm	Production Method
Stainless Steel	Fe	67.4	Atomized
	Cr	17.0	
	Ni	12.0	
	Mo	2.5	
	Si	1.0	
	C	0.1	
NiCrAlY	Ni	76.7	Atomized
	Cr	17.2	
	Al	5.8	
	Y	0.3	
	Zr	92.4	
Yttria Stabilized Zirconia	Y	7.2	Fused
	Fe_2O_3	0.1	
	Trace Oxides	Rest	

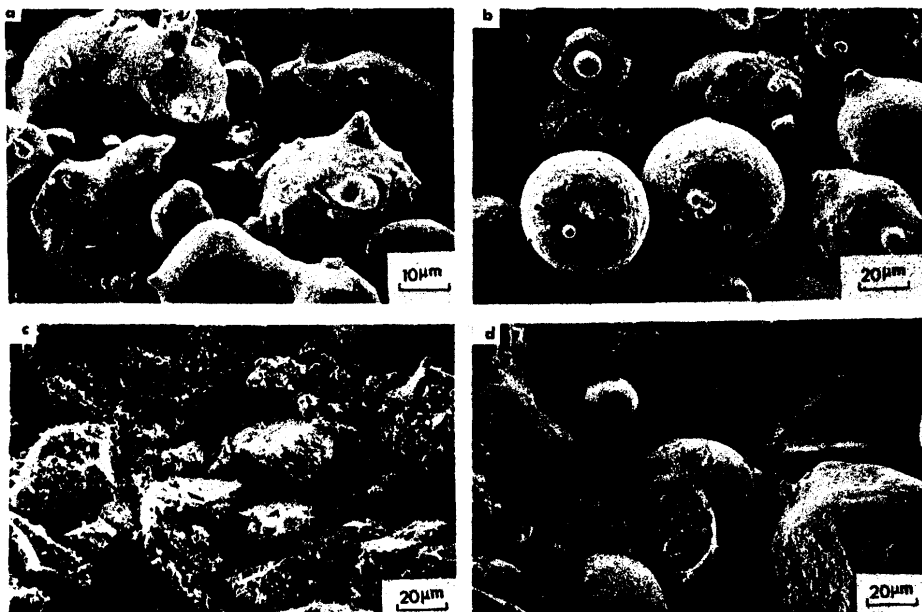


Fig. 1. Morphology of the powders: (a) Stainless steel; (b) NiCrAlY; (c) Yttria stabilized zirconia; (d) YSZ in water quenched state showing partial melting and microcracking.

AE Monitoring of TAT

Tensile adhesion testing was done under a constant force rate of 500 N sec^{-1} with the testing machine in the operation mode of "Load Control". Thus, on unloading there was no crack closure and compression which would have occurred under "Stroke Control". It was possible, therefore, to use the permanent set extension as a measure of the irreversible deformation undergone by the coating.

Acoustic emission was monitored from the initiation of the load and during the subsequent load cycles. Threshold voltages and gains were adjusted so that there were no significant AE counts from a TAT specimen with no coating. Ring-down count rate, RMS voltage, and AE event output were measured during the test, with simultaneous recording of the force vs displacement curve.

The two types of AE spectra that were observed are shown in Fig. 2 and described below.

- 1) The count rate increased gradually to an approximately constant value prior to increasing at failure - i.e., the curves are skewed left (Fig. 2a(i)).
- 2) The count rate increased initially and then decreased to a lower level prior to increasing at failure - i.e., the curves are skewed right (Fig. 2b(i)).

The RMS voltage vs time curves generally exhibited corresponding features with respect to their skewness. There was also a variation in the fluctuation of the RMS voltage, and this is depicted in Fig. 2, where high and low voltage ranges are observed. The event output exhibited similar features to the RMS voltage with respect to their skewness, and, hence, further discussions will be limited to AE counts and RMS voltage. In all of the tests, RMS voltage and count rate increased significantly during the final failure of the coating.

The AE response during a loading cycle is described below. There was a net extension when the specimen was loaded to forces less than the fracture value, and AE signals were produced only during loading and not during unloading. Further loading cycles up to or less than the previous load did not produce further AE signals nor any further extension on unloading. Holding at a constant load produced additional AE counts for some time, and the corresponding RMS voltage was reduced to a low level. When the load level at which the specimen was previously held was exceeded there was an incubation period of a few seconds prior to the re-initiation of an AE signal.

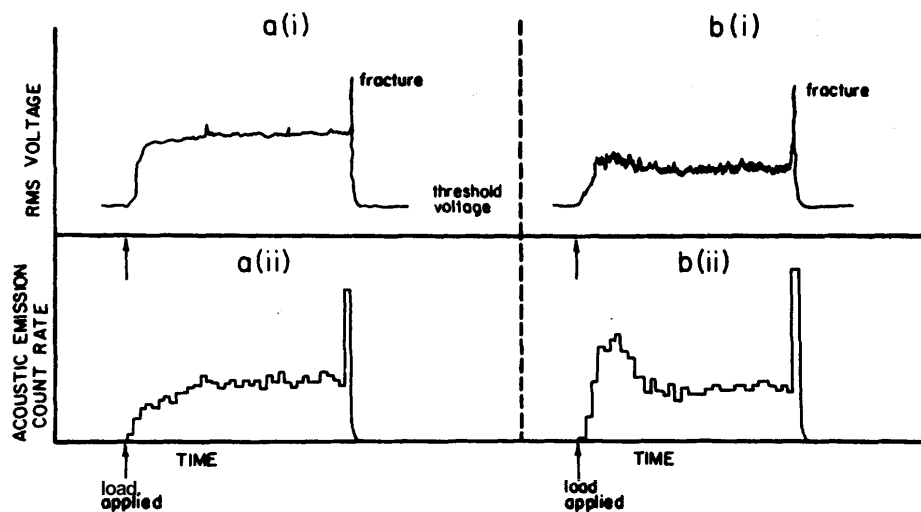


Fig. 2. Two types of AE spectra observed during the TAT: a(i) The AE RMS voltage increases gradually to an approximately constant value prior to increasing at fracture. a(ii) The corresponding AE count rate vs time curve. b(i) The AE RMS voltage increases initially and then decreases to a lower value prior to increasing at failure. Also the RMS voltage fluctuates more than in the case of a(i). b(ii) The AE count rate corresponding to curve b(i).

Table II is a summary of all the TAT tests. Specimens in each category are numbered according to their decreasing bond strengths, with Specimen 1 having the highest bond strength, etc. Likewise "a" has the highest bond strength among the heat-treated coatings.

Stainless Steel Coatings

The cumulative AE counts vs load for stainless steel coatings is shown in Fig. 3. The high slopes at failure are due to high AE counts generated at fracture. Specimens 1, 2 and 3 failed in a cohesive mode, and the AE count plot has a lower slope prior to failure than that during the center part of the test period. The forces up to which the various load cycles were carried out are indicated by the letter "U" (i.e., unloading), while "H" represents "holding" at a specific load. The generation of AE counts at hold, and the subsequent time lag of AE counts in the next loading, results in "steps" in the AE count vs force plot, as can be seen for the case of Specimen 3 and 4. The dashed lines at the 'steps', indicate interpolation of AE counts as if there were no

TABLE II. Summary of AE/TAT Data

Sample Number	Bond Strength Mpa	Net Extension mm	Type of Fracture*	Cumulative AE Counts	Average AE Counts During Test	Shape of Cumulative AE vs Force Plot**
<u>As-Sprayed Stainless Steel Coatings</u>						
1	65.9	0.200	C	88,400	1403	CC
2	59.2	0.025	C	37,550	647	CC
3	51.4	0.035	C	45,350	907	CC
4 [†]	50.4	0.048	C	120,700	2514	CC
5	44.1	0.063	A	14,500	345	L
<u>As-Sprayed YSZ Coatings</u>						
1	34.8	0	A	7,450	226	L
2	30.9	0.094	A	20,680	689	L
3	24.4	0.073	A	7,670	319	L
4	20.8	0.065	A	8,650	433	L
5	18.2	0.071	A	8,900	494	L
<u>Heat-Treated YSZ Coatings</u>						
a	22.9	0.017	A	10,400	472	CV
b	20.8	0.080	A	12,120	606	CV
c	19.2	0.048	A	4,730	262	L
d	17.7	0.070	A	8,200	482	CV
e	15.6	0.005	A	7,200	480	CV
<u>As-Sprayed YSZ + NiCrAlY Coatings</u>						
1	54.8	0.103	M	43,450	945	L
2	36.3	0.040	M	37,700	1077	L
<u>Heat-Treated YSZ + NiCrAlY Coatings</u>						
a	65.4	0.092	C	51,575	819	CC
b	64.4	0.065	C	38,200	670	CC
c	48.6	0.140	M	18,300	425	L

* C - Cohesive; A - Adhesive; M - Mixed (i.e., C + A).

† Sample 4 was flawed.

** Shape is defined with respect to the abscissa as: CC - Concave; CV - Convex; L - Linear.

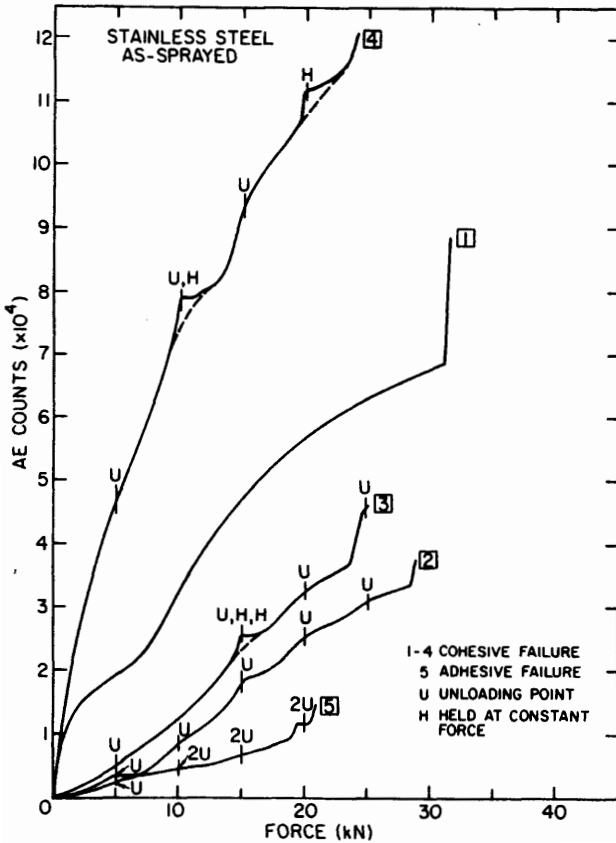


Fig. 3. Cumulative AE counts vs force for as-sprayed stainless steel coatings.

holding at a specific load. The smooth shape of these composite curves indicates that no additional AE was generated as a consequence of the intermittent nature of the test.

The occurrence of a pre-existing crack should be emphasized! (i.e., when a pre-existing crack is present, the AE count-force plot rises abruptly as shown by the curve for Specimen 4.) The RMS voltage showed a large fluctuation, and along with the AE count rate was skewed right. This sample failed at the lowest load among those specimens that failed cohesively and as well generated the maximum AE counts and had a very high average RMS voltage value.

Specimen 5 generated the least AE counts and failed adhesively at a much lower bond strength than the other stainless steel coatings. Also, the curve was not concave to the abscissa as were curves of Specimen 1, 2 and 3, but appeared linear.

Net extension of the coating was measured by the difference in the stroke positions between TAT specimens with and without a coating (shown in Table II). The extension (and as well the AE counts) was higher for those specimens which failed in the cohesive mode. Cohesive failure (Specimens 1 to 3) exhibited interlamellar tearing on both fracture surfaces of the TAT specimen, as shown in Fig. 4a. Fig. 4b indicates the ductile nature of the fracture.

The adhesive fracture surface, on the other hand, was smoother and devoid of any tearing. In some regions, the topology of the grit blasted substrate was revealed on the coating fracture surface.

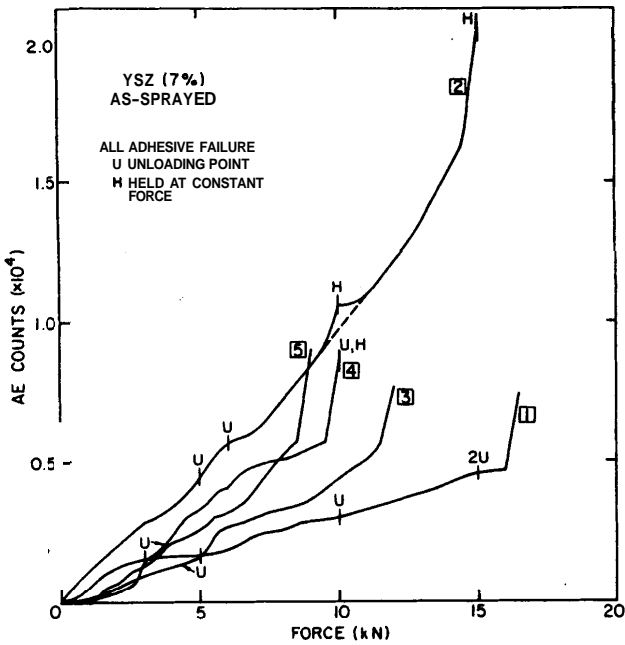
YSZ Coatings

Figs. 5a and b show the plot of AE counts vs force for the yttria-stabilized coatings in the as-sprayed and heat-treated conditions. Heat treatment reduced the bond strength and the average count rate, during the TAT increased slightly (Table II). Also, the AE count-force curves were convex towards the abscissa and failure counts were higher than for the as-sprayed coatings. The RMS voltage fluctuations were larger for those coatings which yielded at higher counts.

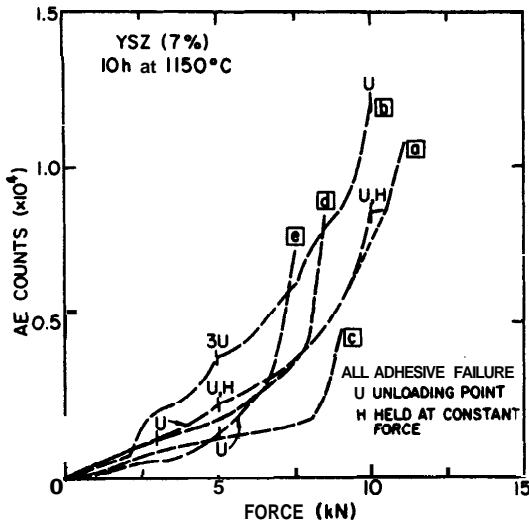
As-sprayed YSZ coatings (Specimens 2 to 5) showed a greater net extension when they yielded more AE counts and higher fluctuations in RMS voltage. Specimen 1 exhibited a low RMS fluctuation and very low average AE count rate and this correlated with a negligible net extension. Heat-treated coatings showed similar correlation of net extension with RMS fluctuations, but no correlation with AE counts.



Fig. 4. Cohesive fracture of as-sprayed stainless steel coating: (a) Area revealing interlamellar tearing; (b) magnified image indicating ductile fracture.



(a)



(b)

Fig. 5. Cumulative AE counts vs force curves for: (a) As-sprayed YSZ coating; (b) heat-treated YSZ coating.

Fracture surfaces of both the as-sprayed and heat-treated coatings were all adhesive in nature. Optical microscopic examination showed a uniform texture of the fracture surfaces with no tearing, as in the case of the stainless steel coatings which failed adhesively. The adhesive fracture surfaces (i.e., the substrate surface and the corresponding support bar-attached coating surface) of the as-sprayed and heat-treated specimens did not exhibit the same features. The common feature was that both series of specimens revealed sections of the ceramic coating on the substrate surface, as well as regions of the substrate. However, the mating fracture surfaces of the as-sprayed coating showed regions of the detached substrate, which appeared as well defined gray-metallic areas. The heat-treated YSZ fracture surface, on the other hand, did not exhibit these regions but showed signs of incipient melting and densification of the ceramic.

SEM fractography allowed the microscopic nature of the cracking process to be followed. The fracture surfaces of the coatings (as-sprayed and heat-treated) which remained on the support bar after a TAT reflected the topology of the grit-blasted substrate (Fig. 6a). The substrate fracture surface of the as-sprayed coating revealed areas of the grit-blasted substrate and regions where YSZ particles (or parts and groups of particles) were firmly attached to the substrate. The particle edges showed a brittle fracture morphology. The substrate fracture surface of the heat-treated samples, on the other hand, showed incipient melting and clusters of small spherical particles (Fig. 6b). EDA of these particles showed the presence of both Zr and Fe. Precise concentration ratios were difficult to estimate due to the small size of the particles and the low resolution of the electron microprobe analyzer.

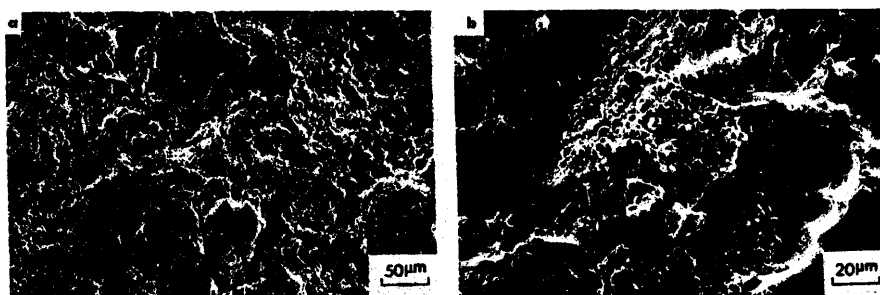


Fig. 6. (a) Adhesive fracture surface (typical of both the as-sprayed and heat-treated YSZ coatings) reflecting the topology of the grit blast substrate. (b) Substrate fracture surface of the heat-treated YSZ coatings revealing incipient melting and with clusters of small spherical particles on it.

YSZ + NiCrAlY Coatings

Yttria-stabilized zirconia, with the incorporation of a NiCrAlY bond coat, had higher bond strengths and yielded higher average AE counts, both in the as-sprayed and heat-treated conditions, as compared to the YSZ coatings (Table II and Fig. 7). The bond strength of the YSZ + NiCrAlY coatings increased after heat treatment. The AE counts vs force response was linear for the as-sprayed coatings (curves 1 and 2 of Fig. 7) and curved for the heat-treated coatings (curves a and b). Optical microscopic examination of the as-sprayed YSZ + NiCrAlY coatings indicated a "mixed" mode of failure, where fracture occurred mostly between the YSZ layer and the NiCrAlY bond coat and partly between the NiCrAlY layer and the substrate. Specimen "c", of the heat-treated coatings, unlike "a" and "b" specimens which fractured cohesively, failed at the substrate bond coat interface (adhesive failure) and also through the YSZ coating (cohesive failure).

Scanning electron microscopy of the as-sprayed coatings was used to characterize the morphology of adhesive fracture between YSZ and NiCrAlY. Fig. 8a shows the fracture appearance of the

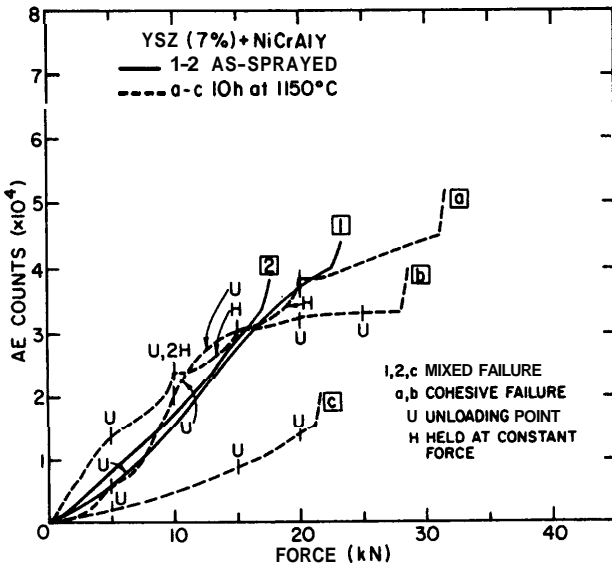


Fig. 7. Cumulative AE counts vs force curves for both the as-sprayed and heat-treated YSZ + NiCrAlY coatings.

coating which remains on the support bar after the TAT, and it can be seen that the topology compliments the coating surface structure. There was also more cracking than in the case of coatings without bond coat (Fig. 8a). Fig. 8b shows the NiCrAlY side (i.e., substrate side) of the adhesive fracture showing the crack free NiCrAlY matrix with fractured YSZ particles embedded in it. After heat treatment, the fracture changed to the cohesive mode, as shown in Fig. 8c. This fractograph of the coating on the support bar shows interlamellar tearing similar to that of stainless steel coatings. However, the fracture appearance of the ceramic appears brittle rather than ductile, as in the case of the metal coating. The substrate side for this cohesive fracture, Fig. 8d, shows brittle-fractured particles of YSZ.

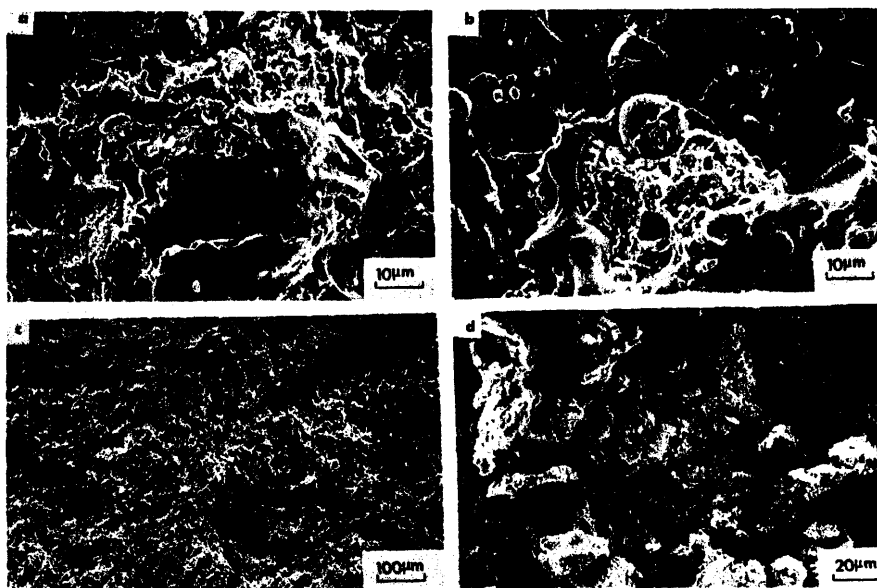


Fig. 8. (a) Adhesive fracture surface of YSZ + NiCrAlY coating showing topology complimentary to bond coat surface and showing a lot of cracking; (b) NiCrAlY side of the above fracture showing crack free NiCrAlY matrix with a brittle-fractured YSZ particle embedded in it. (c) Cohesive fracture of the YSZ + NiCrAlY coating showing lamellar tearing; (d) magnified image of a part of Fig. (c) showing the brittle nature of the fracture.

DISCUSSION

An important feature of these results is the correlation of the AE data with the mechanical behavior of the coatings. Fig. 9 shows that different fracture modes are characterized by their average AE count rate during TAT, with adhesive failure having a lower average AE count rate. On consideration of failure mechanisms, this behavior is to be expected, since coatings which fail in a cohesive manner exhibit a high degree of deformation in the form of interlamellar tearing, indicating greater cracking and, hence, higher average AE counts. In addition, metallic coatings, such as stainless steel and NiCrAlY bond coat, undergo plastic deformation and, thus, have a greater average AE count rate: See Table II.

The shape of cumulative AE vs force plot also corresponds to the mode of fracture. As can be seen from Table II, all cohesive fracture resulted in concave AE plots with respect to the abscissa, indicating that more AE is generated during the beginning of the test than towards the end. This in turn indicates more cracking during the initial portion of the test: since AE was generated only on loading and when there was net extension. The cohesive

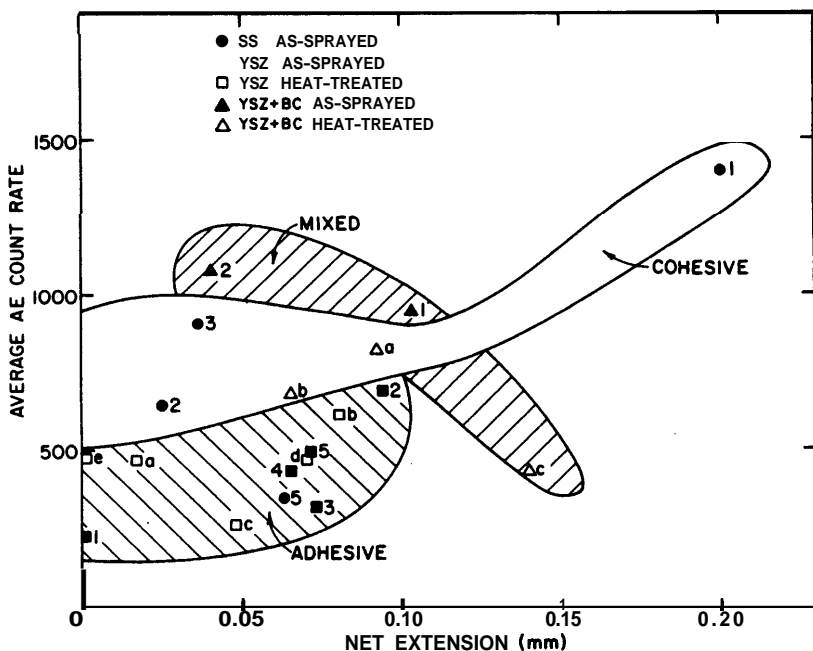


Fig. 9. Average AE count rate plotted vs net extension for the indicated coatings showing regions of different fracture modes.

fracture surfaces show a considerable interlamellar tearing, indicating crack generation at various nuclei. These initial cracks combine together towards the end of the TAT, resulting in a decrease of the AE count rate. The analysis is complicated due to cracks acting as acoustic attenuator^{9,10}.

Heat-treated YSZ coatings failed adhesively and had a lower bond strength than the as-sprayed coatings and incipient melting of the interface resulted in a smooth fracture surface. These coatings showed a convex AE plot indicating that more AE counts were generated towards the end of the TAT. Thus, most of the energy in the heat treated coating was released toward the end of the test as is also shown by their higher counts at failure than the as-sprayed YSZ coatings.

The as-sprayed YSZ coatings which failed in an adhesive manner showed considerable fractured YSZ particles embedded in the substrate. YSZ with NiCrAlY bond coat, both in the as-sprayed and heat-treated conditions, failed in a mixed mode and showed regions of fractured YSZ particles embedded in the NiCrAlY surface; Fig. 8(b). Thus, all coatings had regions of cohesive coating fracture and regions of adhesive interfacial delamination. This combination of fracture modes results in a linear AE plot and appears to be a linear combination of the concave plot of the purely cohesive mode and the convex plots of the purely adhesive mode. But the mixed mode fracture does not necessarily have an intermediate average AE rate, and reasons for this are unclear. It could be that the mixed mode, having a more tortuous fracture surface, resulted in greater cracking and hence higher average AE counts.

A plot of cumulative AE shows a parabolic correlation with the bond strength (Fig. 10). This is similar to the result of previous work⁸ and shows that higher bond strength results in greater cracking and hence higher AE counts. But no correlation was found between net extension, bond strength and average AE count rate. This is surprising since an increase in net extension usually indicates an increase in the bond strength (or yield point) when the Young's modulus is assumed to be constant. This behavior may arise from the large statistical variation of bond strength in any group of tensile adhesion tests. It is likely that the net-extension depends on where the delamination occurs with respect to the interface. That is, failure which occurs closer to the coating-substrate interface will not experience as great a net extension as when failure requires bending of the individual lamellae.

CONCLUSIONS

Acoustic emission was monitored during Tensile Adhesion Testing of stainless steel, YSZ and YSZ + NiCrAlY plasma-sprayed coatings. The latter two coatings were tested both in the as-sprayed

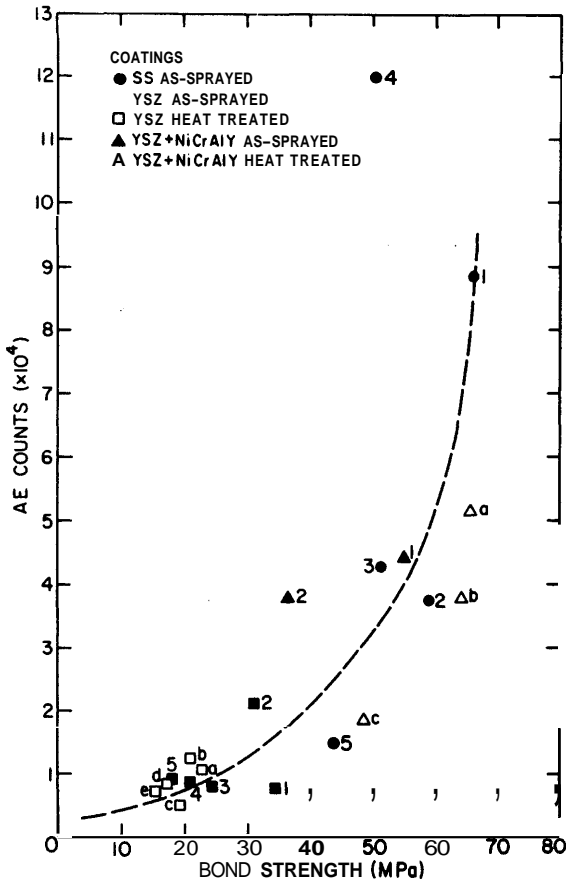


Fig. 10. Cumulative AE counts vs bond strength for all the coatings.

condition and after heat treatment of 10 hours at 1150°C. The AE response of these coatings correlated with their bond strength and fracture surface morphology. Heat treatment decreased the bond strength of YSZ coatings but increased it for the YSZ + NiCrAlY coatings. Also heat treatment altered the type of fracture and changed the characteristics of the generated AE. Extent of strain deformation and average AE count rate of the coatings depended on the type of fracture. Results show that AE can differentiate between different fracture modes and has potential for fundamental coating failure and adhesion studies.

REFERENCES

1. I.A. Fisher, "Variables Influencing the Characteristics of Plasma-Sprayed Coatings", *Int. Metall. Revs.*, 17, 117-129 (1972).
2. S. Secura, "Two-Layer Thermal-Barrier Systems for Ni-Al-Mo

- Alloy and Effects of Alloy Thermal Expansion on System Life", Am. Ceram. Soc. Bull., 61 (2) 256-262 (1982).
3. R. J. Bratton, S. K. Lau and S. Y. Lee, "Evaluation of Present Thermal Barrier Coatings for Potential Service In Electric Utility Gas Turbines", NASA Contract Rep. NASA CR-165545 (1982).
 4. ASTM C633-69, American Society for Testing and Materials Standard Titled "Standard Method of Test for Adhesion or Cohesive Strength of Flame-Sprayed Coatings".
 5. F. J. Hermanek, "Determining the Adhesive/Cohesive Strength of Thin Thermally Sprayed Deposits", Weld. J. (Miami, Fla.) 57 (11) 31-35 (1978).
 6. R. L. Apps, "The Influence of Surface Preparation on the Bond Strength of Flame-Sprayed Aluminum Coatings on Mild Steel", J. Vac. Sci. Technol., 11 (4) 741-746 (1974).
 7. W. Swindlehurst, "Acoustic Emission - I: Introduction", Non. Destr. Test. 6 (3) 152-158 (1973).
 8. N. R. Shankar, C. C. Berndt and H. Herman, "Failure and Acoustic Emission Response of Plasma-Sprayed $ZrO_2-8 \text{ wt} \% Y_2O_3$ coatings" 6th Annual Conference on Composites and Advanced Ceramic Materials, Cocoa Beach, Florida, Jan. 17-21 (1982).
 9. H.N.G. Wadley, C. B. Scruby and J. H. Speake, "Acoustic Emission for Physical Examination of Metals", Int. Met. Revs., 25 (2) 41-64 (1980).
 10. R. L. Cox, D. P. Almond and H. Reiter, "Ultrasonic Attenuation in Plasma Sprayed Coating Materials", Ultrasonics, 19 (1) 17-22 (1981).